Aerodynamic Steering of a 10 cm High-Speed Running Robot

N.J. Kohut† D. Zarrouk* K. C. Peterson* and R. S. Fearing*

***Abstract*— Turning while running at high speeds remains a difficult task for legged robots, but this capability is crucial for maneuvering quickly in a real-world environment. In this work we present a 10 cm long novel robot, SailRoACH, the first running robot that uses aerodynamic forces to turn. We present a scale analysis of aerodynamic steering, showing this steering method is most effective for small robots. Modeling and simulations were performed, and validated with experiments, that showed the robot is capable of stably turning in a 1.2 m radius at 1.6 ms^{-1}. We also show that aerodynamic steering is superior for high speed turns at high forward velocity, compared to existing methods. Additionally, aerodynamic steering allows us to introduce a constant yaw disturbance to the robot. This is useful for studying legged locomotion, and is difficult to achieve otherwise.**

I. Introduction

The mobility of a legged robot depends on its ability to both turn and run straight at high speeds. High speed locomotion has been explored in [1] [3] [16], and legged robots use many methods for turning, such as leg kinematics [14], leg forces [11], or inertial actuators [7]. These methods allow the robot to turn, but also often do not allow for high yaw rates while maintaining high running speeds. Aerodynamics are a relatively unexplored realm for turning in running robots, although they have been used for other functions.

Aerodynamics are of course a crucial aspect of flying robots [9][17][15]. Other non-flying robots have exploited aerodynamics for a performance advantage. DASH+Wings [13] showed improved performance in forward running speed and stability compared to its wingless version, while the EPFL jumpglider [8] also employs aerodynamics to increase its mobility. Little work has been done however, on aerodynamic surfaces in running robots used for purposes other than flight or gliding. The VelociRoACH [5], is a notable exception, and uses a large roll stabilizer with aerodynamic damping to increase its stability while running at high speeds. To the authors' knowledge, steering of a legged robot using aerodynamic forces while the robot runs over the ground has not been explored.

In addition to its use as a steering method, the sail may be used to introduce a constant yaw disturbance to the robot. This could be useful for the study of legged locomotion, for example, studying resistance to construction biases.

This material is based upon work supported by the National Science Foundation under IGERT Grant No. DGE-0903711 and by the Army Research Laboratory under the Micro Autonomous Systems and Technology Collaborative Technology Alliance .

Corresponding author: kohut@stanford.edu, † Dept. of Mechanical Engineering, University of California, Berkeley

∗ Dept. of Electrical Engineering and Computer Sciences, University of California, Berkeley

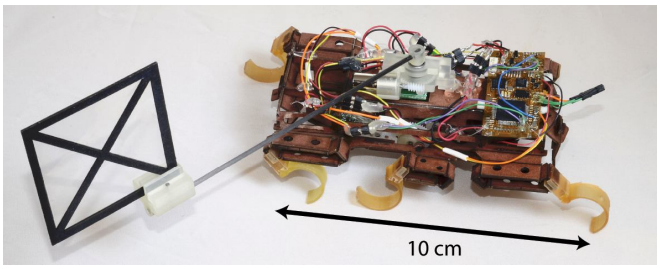

Fig. 1. SailRoACH runs at over 22 body lengths per second and can use aerodynamic forces from its sail to turn.

The sail can also be actuated dynamically, causing a rapid change in body orientation through inertial effects. Body reorientation through inertial effects in lizards has been examined in [10], and [4] explores inertial redirection of aerodynamic forces in hawkmoths. Terrestrial inertial turning in legged robots was explored in detail in [7], but will be expanded on here by showing that this can also be accomplished on high friction surfaces. This also demonstrates that a single actuator can be used for multiple turning modes. This multi-functionality is especially valuable at small scales where degrees of freedom and actuators cannot be easily added to a robot.

II. Robot Design

A. SailRoACH

SailRoACH, shown in Fig. 1, is a six legged robot, 10 cm long, with a mass of 45 grams. Its legs are driven by two 7 mm brushed DC motors, one for the left set of legs and the other for the right. Another 7 mm brushed DC motor drives the sail boom through a custom designed transmission that allows for 360 degree rotation. The chassis is constructed using the Scaled Composite Microstructures (SCM) process [6], and is similar in mechanical design to the VelociRoACH [5] and TAYLRoACH [7].

B. Sail Design

The sail is constructed of cardboard and PET using the SCM fabrication process. It forms a 50 mm x 50 mm flat plate and weighs 0.7 grams. The carrier pieces that attach to the sail weigh a combined 2.7 grams and are discussed in Section II-D.

C. Sail Transmission Design

The sail is driven through a 7.5 gram 3D printed[1] transmission that allows for unlimited rotation. Attached to the

[1] http://printin3d.com/3d-printers

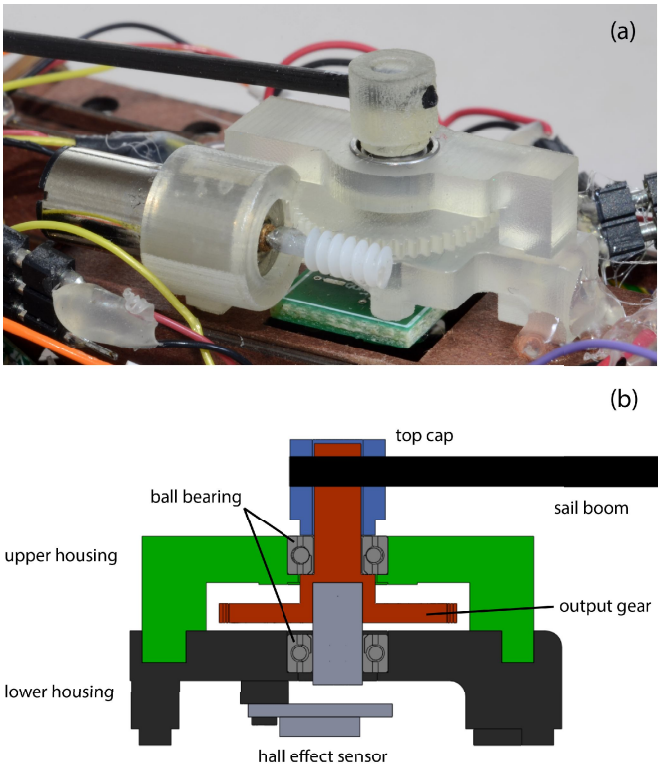

Fig. 2. (a) The transmission mounted on SailRoACH. (b) A CAD rendering of the transmission shown in section view here. The driving motor and worm gear are not shown for clarity.

transmission is a 14-bit AMS AS5048B-HTSP-500 Hall Effect absolute position encoder, providing feedback on the sail position. The sail is mounted on a 12 cm long carbon fiber rod.

Compactness and light weight are key attributes for an actuator on a robot at this size scale. To provide bearing support without limiting the sail's range of motion, the transmission housing is composed of an upper and lower piece. The lower housing holds the motor, the Hall effect sensor, and a ball bearing. The upper housing press fits into the lower housing, locates the transmission's output gear, and also holds a ball bearing. The double bearing supported output gear sits in between the upper and lower housing, and holds a diametrically polarized magnet used for Hall effect position sensing. A top cap joins the sail boom to the output gear, and provides a thrust constraint. The output gear is located such that it rotates while touching the moving part of the ball bearing, meaning there is very little friction in the system. This allows for rapid, efficient movement of the sail if desired. A section view of the transmission can be seen in Fig. 2.

The transmission is driven by a worm gear on the motor. This allows for a large gear reduction with only a single gear, making the design much more compact. Due to the high friction properties of the worm gear, it is difficult to back drive. This significantly reduces the energy required to hold the sail in a static position.

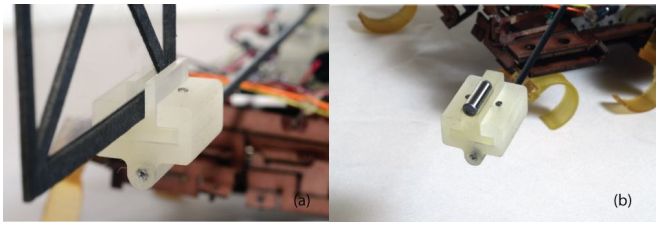

Fig. 3. (a) The sail element fitted at the end of the boom, held with two pins. (b) A ballast element is used for control experiments. The change in center of gravity is preserved, without accompanying aerodynamic effects.

D. Interchangeable Ballast

It is important to have an experimental control for aerodynamic experiments. A 3D printed "carrier" piece permanently attaches to the carbon fiber boom, and can be loaded with the sail, a non-aerodynamic ballast, or potentially other end pieces, as shown in Fig. 3. The sail or ballast slots into the carrier piece with a slip fit, and is secured with two pins that can be easily removed.

E. Power, Communication, and Control Hardware

The power, communication, and control hardware are substantially similar to that presented in [7] and will not be discussed at length in this paper. The legs are equipped with Hall effect incremental encoders that feed a 1 kHz control loop, ensuring phase locking between the left and right sides, allowing for an alternating tripod gait. The sail uses PID control to regulate its position, using feedback from the Hall effect absolute position encoder. A 3-axis MEMS gyroscope provides yaw, pitch, and roll rates. Motion commands are sent from a host system, and then executed autonomously.

III. Aerodynamic and Legged Running Models

A. Aerodynamic Force Modeling and Wind Tunnel Measurements

The sail can induce a moment on the robot through aerodynamic drag and lift forces. We assume that the aerodynamic force normal to the sail follows the equation:

$$F_n = (1/2)\rho C_n A v^2 \tag{1}$$

where ρ is the density of air, C_n is the non-dimensional aerodynamic coefficient, A is the surface area of the sail, v is the wind speed, and F_n is the force normal to the sail.

To test this model, and determine the aerodynamic coefficients, we gathered data in a wind tunnel (Aerovent, Inc.) with a square cross section of 0.61 m^2 using an ATI Nano-17 6-axis force transducer. The yaw moment produced by the sail on the robot is determined by F_n.

$$T = F_n \cdot l \tag{2}$$

where T is the torque, and l is the distance from the sail's center of pressure to the center of mass of the robot. It is assumed that the center of pressure is the geometric center of the sail.

Fig. 4 shows the measured force perpendicular to the sail at wind speeds from 0 to 2.5 ms^{-1} in 0.25 ms^{-1} increments

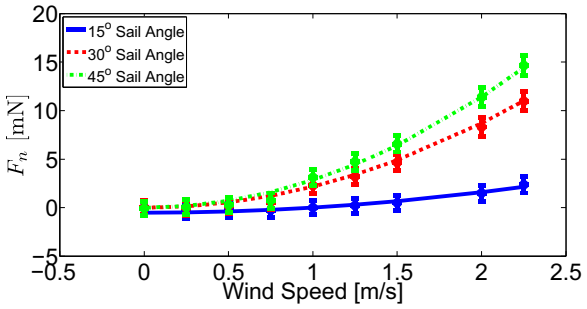

Fig. 4. Wind tunnel results for 15 °, 30 °, and 45 ° sail angles. 60 ° and 75 ° sail angle data are omitted for clarity. The data points were obtained from the wind tunnel, shown with error bars representing ± 1 s.d. The lines represent the model from Eq. 1 using the values for C_n shown in Table I.

and at angles of attack from 0° to 75° in 15° increments. Fig. 4 only shows data from 15°, 30° and 45° for clarity, as 60° and 75° were not appreciably different from the 45° measurements.

Along with the normal force on the sail, the drag force also affects the ability of the robot to turn by limiting the forward velocity, and can be calculated by:

$$\begin{bmatrix} \cos(\alpha) & \sin(\alpha) \\ -\sin(\alpha) & \cos(\alpha) \end{bmatrix} \begin{bmatrix} F_t \\ F_n \end{bmatrix} = \begin{bmatrix} F_d \\ F_l \end{bmatrix} \quad (3)$$

where α is the sail angle, F_d is the drag force, F_l is the lift force (lateral to the robot), and F_t is the force tangential to the sail. We assume that these forces also follow the model described in Eq. 1.

Table I shows the yaw moment and drag coefficients across a range of sail angles based on fitting the data from our wind tunnel experiments to Eq. 1. For the best aerodynamic turning, the yaw moment coefficient should be maximized and the drag coefficient minimized. An angle of 30 ° shows a good operating point, and was used for experiments.

TABLE I
YAW MOMENT AND DRAG COEFFICIENTS

Sail Angle	C_n	C_d	$\frac{C_n}{C_d}$
15 °	0.27	0.34	0.79
30 °	1.20	0.85	1.41
45 °	1.60	1.28	1.25
60 °	1.54	1.41	1.09
75 °	1.57	1.54	1.02

B. General Description of the Model

In our simplified model we assume that the robot consists of a main body and six actuated flexible legs which rotate around their hips providing thrust (see Fig. 5) and use [18] to model the dynamics. The aerodynamic forces acting on the tail are estimated using Eq. 1 as described in section III-A. The robot runs with an alternating tripod gait consisting of a left tripod (LT, legs 1,4,5) and a right tripod (RT, legs 2,3,6), as seen in Fig. 5. A step begins when a tripod contacts the surface and ends when it disengages, marking the beginning

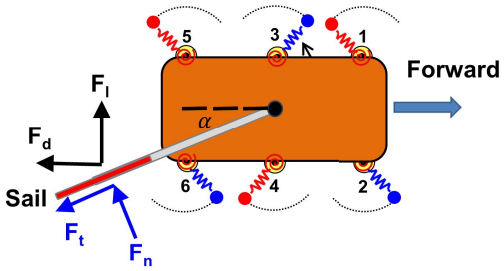

Fig. 5. A diagram of the model. LT is comprised of legs 1,4,5 and RT is made of legs 2,3,6.

of the next step. A cycle is comprised of two successive steps LT and RT.

We assume that the robot has a rigid body with a mass m and inertia moment I_b and that, due to well tuned legs, vertical oscillations are small, and thus the dynamic model of the robot is restricted to the horizontal plane. The mass of the legs constitutes a small percentage of total weight and is therefore neglected in this analysis. The center of mass (COM) of the robot without the sail is the geometrical center of the robot, but the COM shifts towards the direction of the sail. In this sliding spring leg (SSL) model [19][18], the legs are rigid against bending but compliant along their length with a spring constant k_l. At their hips, the legs are attached to the motor by a torsional spring whose stiffness is k_r.

We assume that at the beginning of a step, the robot places its unloaded legs over the surface with no impact and contacts the surface at the leg tips only. To model the friction between the robot and surface, we adopt the standard Coulomb model of friction. The Coulomb model explicitly defines the maximum friction force acting on the tip of the legs as a product of the coefficient of friction and the normal force. As in [18], the equations of motion of the robot are directly simulated in Matlab, allowing for the calculation of robot speed, position, and other variables. The results of the simulation, compared with experimental data, are shown in Section IV, Fig. 6, for a robot running at a nominal speed of 2 ms^{-1} for 3 seconds, while equipped with the sail. Simulations performed without the sail but with a displacement in center of mass showed nearly straight running, with a turning radius of 46 m.

IV. EXPERIMENTAL RESULTS

A. Aerodynamic Steering

SailRoACH was run forward at a 21 Hz stride frequency for 60 strides with its sail held at constant position. As a control, the same experiments were done with the sail replaced by a ballast of the same weight but minimal aerodynamic properties (refer to Fig. 3). Results were recorded using a Vicon motion capture system[2]. Eight to fourteen trials were performed for each configuration. When the robot first starts running, there is a transient phase where its heading changes

[2]http://www.vicon.com/

TABLE II

STEADY STATE YAW RATE AND SPEED, 21 HZ STRIDE FREQ.

Configuration	$\dot{\theta}$ [$^\circ s^{-1}$]	Speed [ms^{-1}]
Sail Left	51 ± 19	2.02 ± 0.10
Ballast Left	2 ± 16	1.86 ± 0.12
Sail Center	0 ± 13	2.28 ± 0.05
Ballast Center	-15 ± 22	2.09 ± 0.05
Sail Right	-73 ± 23	1.84 ± 0.19
Ballast Right	-25 ± 19	1.99 ± 0.10
VelociRoACH [5]	–	∼2.0

due to the stochastic nature of the surface contact. All measurements of yaw rate and speed are made at steady state, and this transient effect is neglected. The paths described by the robot while running are shown in Fig. 6. Even at steady state, there is some variation to the paths, as the robot is running open loop, and small variations in surface contact can lead to path variations.

When equipped with the ballast, the center of mass is shifted, but aerodynamic effects are negligible. This does not significantly affect the path of the robot. The robot turns right slightly in many of these trials, irrespective of ballast position. This is likely due to a slight asymmetry in the robot's hand assembled structure. This also explains why the simulation overestimates left turns while underestimating right turns.

When the sail is placed at an angle, the robot turns due to the aerodynamic torque on the body. With the sail 30 degrees left, the robot turns at an average of 51$^\circ s^{-1}$ while running at steady state. When placed at 30 degrees right, the robot turns at an average of -73$^\circ s^{-1}$. The ballast performs significantly worse, at 2$^\circ s^{-1}$ and -25$^\circ s^{-1}$ for left and right placement, respectively. These measurements can also be found in Table II.

When the ballast is positioned at zero degrees (straight back), the turning rate is -15$^\circ s^{-1}$, compared to 0$^\circ s^{-1}$ when the sail is positioned at zero degrees. This indicates that the sail provides a stabilizing torque while the robot runs forward.

B. Forward Speed

For maneuverability, maintaining high speed running is important. The sail mechanism constitutes 23% of the total robot weight, and adds aerodynamic drag, which may slow the robot down. Experimental evidence however, does not show this. When running forward with the sail or ballast at an angle, the steady state speed of the robot was between 1.84 and 2.02 ms^{-1}, as shown in Table II. When the sail or ballast was positioned rearward, the sail produces slightly higher speeds, at 2.28 ms^{-1}versus 2.09 $ms^{-1}$for the ballast. This is mostly likely due to the stabilizing effect of the sail, which rejects yaw disturbances that may slow the robot down.

Haldane et al. [5] measured the speed of this robot chassis without an additional sail mechanism, and reported approximately 2 ms^{-1}at 21 Hz running frequency. The robot is not power limited, but limited by stability. One possibility for this performance difference is that the extra inertia and aerodynamic stabilizing torque of the sail may reduce the rotational energy of the body as the robot runs forward, ensuring more consistent footfalls.

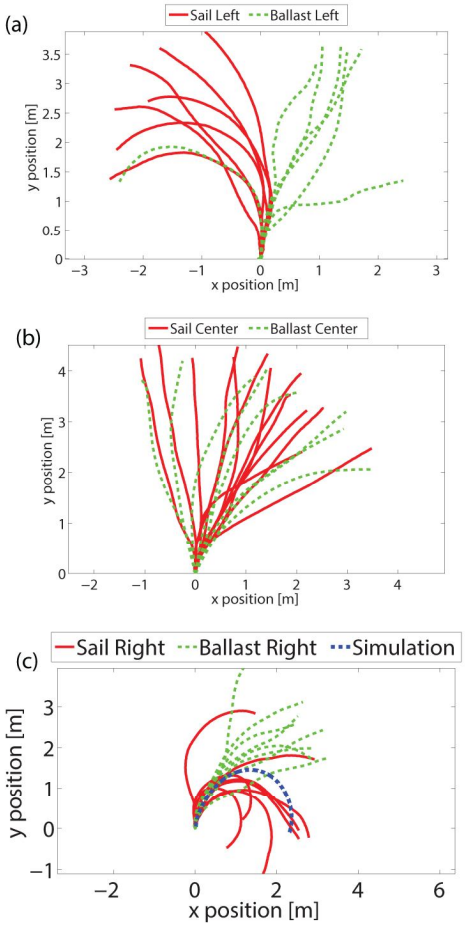

Fig. 6. (a) The paths of the robot when the sail or ballast is held 30 degrees to the left of center. (b) The paths of the robot when the sail or ballast is held at center. (c) The paths of the robot when the sail or ballast is held 30 degrees to the right of center. Simulation results for the sail held 30 degrees right are shown in the blue dotted line. Placing the sail at an angle produces a turning moment, while placing the sail directly behind the robot produces a stabilizing moment.

V. COMPARISON OF STEERING METHODS

Many methods have been demonstrated that allow legged robots to turn, but few are effective at high speeds. McClung [11] defines a turning performance parameter that measures the ability to both turn and run forward:

$$K = \dot{\theta} v \tag{4}$$

where $\dot{\theta}$ and v are the simultaneous yaw rate and speed. We will use this to characterize various turning methods.

A. Differential Drive

The OctoRoACH [14] turns by moving legs on one side faster than the other. This causes the outside of the robot to move farther than the inside, producing a turn. The OctoRoACH is able to make 90$^\circ s^{-1}$ turns while running forward at 0.4 ms^{-1}. This turning method is effective, but

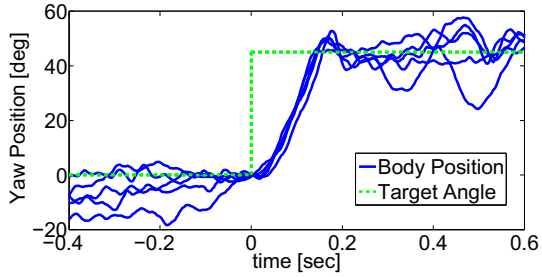

Fig. 7. Heading of SailRoACH as a function of time during inertial turning. Before $t = 0$ no steering control is employed. At $t = 0$ a 45 degree turn is commanded using inertial exchange.

precludes high speed running. The leg sides are not in phase with each other, an alternating tripod gait cannot be used, and the force produced by the legs cannot be coordinated, limiting the top speed.

B. Differential Leg Phasing

The XRL robot uses differential leg phasing and a modified Buehler clock to turn [12]. This mode has the advantage of maintaining an alternating tripod gait, but requires a high degree of intra-stride control, and uses 6 motors. It is possible that using two motors could also accomplish similar behavior. As shown in [12], the XRL can turn at $8°s^{-1}$while running forward at 0.18 ms^{-1}.

C. Modified Leg Kinematics

The SPRAWL family of robots turns effectively while running forward. iSprawl is a hexapedal robot that can change the angle of its middle legs. This causes a yaw moment, turning the robot. At 6Hz stride frequency, iSprawl is able to run forward at 0.5 ms^{-1}while turning at approximately $40°s^{-1}$[11].

D. Inertial Turning

TAYLRoACH [7] is able to turn rapidly on low friction surfaces using a tail to induce a quick exchange of angular momentum. This generates a yaw rate of $360°s^{-1}$ while running forward at 0.3 ms^{-1}. SailRoACH is also able to generate rapid turns using its sail as an inertial mechanism. However, due to SailRoACH employing an alternating tripod gait unlike TAYLRoACH, it is able to turn on high friction surfaces as well. Fig. 7 shows the results of a controlled inertial turn performed on a high friction surface (carpet, $\mu_s \sim 2.0$).

Inertial turns however, generally cannot be executed over multiple strides, whether due to saturation of an actuator or the instability introduced by the actuation. We consider this type of turning transient.

SailRoACH is able to consistently make transient tail inertial $200°s^{-1}$ turns on carpet, while running at 1.8 ms^{-1}. It should be noted that this turn is performed with the same actuator used for the aerodynamic steering. This equips SailRoACH to make quick, sharp turns, or long, wider turns with a single actuator. This behavior is shown in the included video.

E. Aerodynamic Turning

SailRoACH is able to use its sail to generate torques aerodynamically, turning the robot. This turning method is completely decoupled from the legs, meaning an alternating tripod gait can be maintained. Although not as rapid as the inertial turning method, aerodynamic turning can be executed continuously, as long as forward speed is maintained, unlike inertial turning, which requires rapid actuation of a mass and generally takes place only over a short period of time.

Table III shows the maneuverability, K, of each highlighted robot. Many different methods of turning are effective, but aerodynamic and inertial turning allow for high yaw rates and for an alternating tripod gait to be employed, making the product of yaw rate and forward velocity high.

TABLE III

COMPARISON OF TURNING METHODS.

Robot	$K = \dot{\theta}v$ $[°ms^{-2}]$	Transient?
OctoRoACH [14]	36	No
XRL [12]	1.44	No
iSprawl [11]	18	No
TAYLRoACH [7]	108	Yes
SailRoACH(Inertial)	360	Yes
SailRoACH(Aerodynamic)	134	No

F. Scaling of Aerodynamic Steering

Aerodynamic effects are greatly influenced by scale. Here, we examine the effects of scaling on steering aerodynamics, using the characteristic length of the robot, L, as the main scaling factor. The aerodynamic turning moment is given by

$$F_n \sim Av^2 \sim L^2v^2 \tag{5}$$

$$T \sim F_nL \sim L^3v^2. \tag{6}$$

The velocity of the robot also depends on aerodynamic drag force. Robot velocity as a function of resisting force has not been explicitly determined, however, in previous work [18][2] it was found that the speed of locomotion of the robot ascending a slope is a linearly decreasing function of the form

$$V(\lambda) = (1 - c_1 \tan(\lambda))V_o \sim (1 - c_1\lambda)V_o \tag{7}$$

where λ is the slope. For small slope angles, normal force is approximately constant and we assume the speed of the robot is a function of the resisting force, and is of the form

$$V(F) \sim (1 - c_2F)V_o. \tag{8}$$

Then,

$$V(mg\lambda) \sim (1 - c_2mg\lambda)V_o = (1 - c_1\lambda)V_o \tag{9}$$

and

$$c_2mg\lambda = c_1\lambda \implies c_2 = \frac{c_1}{mg}. \tag{10}$$

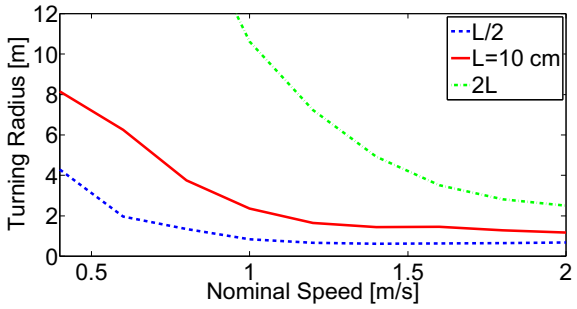

Fig. 8. From simulation, aerodynamic steering is more effective for small robots.

Substituting into Eq. 9 we find that the velocity is a function of the resisting force and the mass of the robot.

$$V(F) \sim \left(1 - \frac{c_1}{mg} F\right) V_o \tag{11}$$

We assume for steady state turning that the tail moment is balanced by the body moment created by the thrust difference on the left and right sides, and for steady state running, that tail aerodynamic drag and foot contact drag forces are balanced by foot thrust. For steady state turning, the outer legs have higher velocity than the inner legs. By assuming, that on a time-average basis, Eq. 11 applies to individual legs, we can predict the difference in velocity/force between left and right sides:

$$V_{A1} - V_{A2} = \left[\left(1 - \frac{c_1}{mg} F_{A1}\right) - \left(1 - \frac{c_1}{mg} F_{A2}\right)\right] V_o \tag{12}$$

$$V_{A1} - V_{A2} = \frac{c_1 V_o}{mg} (F_{A1} - F_{A2}) \tag{13}$$

where F_{A1} and F_{A2} are the forces acting on each side of the robot as a resultant of the aerodynamic torque and drag. The force difference acting on the two sides of the robot is the torque divided by the width w of the robot

$$(F_{A1} - F_{A2}) \sim \frac{T}{w} \sim \frac{L^3}{L} \sim L^2. \tag{14}$$

Substituting Eq. 14 into Eq. 13, and recalling that $m \sim L^3$, the differential velocity is proportional to L^{-1}.

$$(V_{A1} - V_{A2}) \sim \frac{L^2}{L^3} \sim \frac{V_o}{L} \tag{15}$$

Thus, the angular velocity of the robot is inversely proportional to L^2

$$\dot{\theta} = \frac{V_{A1} - V_{A2}}{w} \sim \frac{V_o}{L^2} \tag{16}$$

and the turning radius is

$$R \sim \frac{V_o}{\dot{\theta}} \sim L^2. \tag{17}$$

Simulation results using the model from Section III for robots at different scales are shown in Fig. 8.

VI. Conclusions

SailRoACH is the first running robot that uses aerodynamics to steer. We showed that aerodynamic steering's effectiveness scales inversely with robot size squared, making small robots especially well equipped to employ this method. We also presented an aerodynamic and legged locomotion model that is able to predict the performance of the real robot. SailRoACH is capable of steady state $73° s^{-1}$ turns while running at over 1.8 ms^{-1}. This performance is superior to other existing sustainable turning methods when judged by the maneuverability metric, $K = \dot{\theta} v$. SailRoACH can also make rapid, transient turns by inertial exchange, achieving $200° s^{-1}$ while running forward at 1.8 ms^{-1}. The running speed of the robot was increased from 2.1 to 2.3 ms^{-1} when using the sail directly rearwards, but it did not slow the robot when the sail was angled for turning, compared to mounting the ballast at an angle.

Aerodynamic steering has benefits from a scientific standpoint as well, as it provides a way to introduce a nearly constant yaw disturbance to the robot. This is otherwise difficult and could be useful for studying turning, leg gait, or other dynamic phenomena in the future. As running robots become smaller and faster, aerodynamics will come to play an even larger role in their performance, and consideration of aerodynamic forces and torques may become crucial for stability and maneuverability.

VII. Acknowledgements

The authors thank the Berkeley Animal Flight Laboratory for the use of their wind tunnel. Also thanks to Duncan Haldane for hardware support, Andrew Pullin for mechanical design discussions, and Katherine Cheung for assistance with experiments.

References

[1] P. Birkmeyer, K. Peterson, and R. S. Fearing, "DASH: A dynamic 16g hexapedal robot," in *IEEE Int. Conf. on Intelligent Robots and Systems*, St. Louis, MO, 2009.

[2] P. Birkmeyer, A. G. Gillies, and R. S. Fearing, "Dynamic climbing of near-vertical smooth surfaces," in *IEEE/RSJ Int. Conf. on Intelligent Robots and Systems*, 2012, pp. 286–292.

[3] J. G. Cham, S. A. Bailey, J. E. Clark, R. J. Full, and M. R. Cutkosky, "Fast and robust: Hexapedal robots via shape deposition manufacturing," *The Int. Journal of Robotics Research*, vol. 21, no. 10-11, pp. 869–882, 2002.

[4] J. P. Dyhr, K. A. Morgansen, T. L. Daniel, and N. J. Cowan, "Flexible strategies for flight control: An active role for the abdomen," *The Journal of Experimental Biology*, vol. 216, no. 9, pp. 1523–1536, 2013.

[5] D. Haldane, K. Peterson, F. Bermudez, and R. Fearing, "Animal-inspired design and aerodynamic stabilization of a hexapedal millirobot," in *IEEE Int. Conf. on Robotics and Automation*, May 2013.

[6] A. M. Hoover and R. S. Fearing, "Fast scale prototyping for folded millirobots," in *IEEE Int. Conf. on Robotics and Automation*, Pasadena, CA, 2008.

[7] N. Kohut, A. Pullin, D. Haldane, D. Zarrouk, and R. Fearing, "Precise dynamic turning of a 10 cm legged robot on a low friction surface using a tail," in *IEEE Int. Conf. on Robotics and Automation*, May 2013.

[8] M. Kovac, W. Hraiz, O. Fauria, J.-C. Zufferey, and D. Floreano, "The EPFL jumpglider: A hybrid jumping and gliding robot with rigid or folding wings," in *IEEE Int. Conf. on Robotics and Biomimetics (ROBIO)*, 2011, pp. 1503–1508.

[9] D. Lentink, S. R. Jongerius, and N. L. Bradshaw, "The scalable design of flapping micro-air vehicles inspired by insect flight," *Flying Insects and Robots, edited by D. Floreano, M. Srinivasan, C. Ellington, and J.C. Zuffrey*, p. 185, 2009.

[10] T. Libby, T. Moore, E. Chang-Siu, D. Li, D. Cohen, A. Jusufi, and R. Full, "Tail-assisted pitch control in lizards, robots and dinosaurs," *Nature*, vol. 481, pp. 181–184, 2012.

[11] A. McClung, "Techniques for dynamic maneuvering of hexapedal legged robots," Ph.D. dissertation, Stanford University, 2006.

[12] C. Ordonez, N. Gupta, E. Collins Jr., and J. Clark, "Power modeling of the XRL hexapedal robot and its application to energy efficient motion planning," in *15th Int. Conf. on Climbing and Walking Robots (CLAWAR)*, July 2012.

[13] K. Peterson, P. Birkmeyer, R. Dudley, and R. Fearing, "A wing-assisted running robot and implications for avian flight evolution," *Bioinspiration & Biomimetics*, vol. 6, no. 4, p. 046008, 2011.

[14] A. Pullin, N. Kohut, D. Zarrouk, and R. Fearing, "Dynamic turning of 13 cm robot comparing tail and differential drive," in *IEEE Int. Conf. on Robotics and Automation*, May 2012.

[15] E. R. Ulrich, D. J. Pines, and J. S. Humbert, "From falling to flying: the path to powered flight of a robotic samara nano air vehicle," *Bioinspiration & Biomimetics*, vol. 5, no. 4, p. 045009, 2010.

[16] J. Weingarten, G. A. D. Lopes, M. Buehler, R. E. Groff, and D. Koditschek, "Automated gait adaptation for legged robots," in *IEEE Int. Conf. on Robotics and Automation*, vol. 3, April-1 May, 2004, pp. 2153–2158 Vol.3.

[17] R. J. Wood, "The first takeoff of a biologically inspired at-scale robotic insect," *IEEE Trans. Robotics*, vol. 24, no. 2, pp. 341–347, April 2008.

[18] D. Zarrouk and R. Fearing, "Cost of transport of a dynamic hexapedal robot," in *IEEE Int. Conf. on Robotics and Automation*, May 2013.

[19] D. Zarrouk, A. Pullin, and R. Fearing, "In-plane dynamics of compliant hexapedal running," (submitted).